Acta Mechanica Solida Sinica (2023) 36:143–155
https://doi.org/10.1007/s10338-022-00360-1

Singularities of Three-Dimensional Cubic Piezoelectric Quasicrystal Composite Wedges and Spaces

Xiang Mu[1,2] · Ting Cao[1] · Wenshuai Xu[3,4] · Zhaowei Zhu[1] · Taiyan Qin[1] · Liangliang Zhang[1] · Yang Gao[1]

Received: 30 June 2022 / Revised: 14 September 2022 / Accepted: 15 September 2022 / Published online: 4 November 2022

Abstract
In this paper, the planar problems of three-dimensional (3D) cubic piezoelectric quasicrystal composite wedges and spaces are investigated. The study focuses on the singular behaviors of interface corner and interface crack of composite wedges and spaces. To research the stress singularities, the stress function is assumed to have the exponential form. Based on the Stroh formalism and Barnett–Lothe matrices, we derive a crucial matrix concerned with material properties and wedge angle and obtain the transcendental equation determining the singular orders by simple multiplication of the crucial matrix. Numerical examples of the singular orders are given for some general cases including single, bi-material, and tri-material wedges and spaces under different boundary conditions. The correctness of numerical results is verified by comparison with the existing results of piezoelectric material. Numerical results show that the phonon field, phason field, electric field, material properties, and boundary conditions have great influences on singularities.

Keywords Composite wedges · Stroh formalism · 3D cubic piezoelectric quasicrystals (QCs) · Singular orders

1 Introduction

Quasicrystals (QCs) with multi-physics fields, such as the phonon field and phason field, were firstly discovered in 1982 by Levine and Shechtman [1]. The phonon field in QCs resembles that in crystals, and its gradient depicts the changes in the volume and shape of a cell. The gradient of the phason field is in terms of local rearrangements of atoms [2]. Unlike crystals and non-crystals, QCs possess quasi-periodic atomic configurations, causing non-crystallographic rational symmetry, e.g., fivefold, eightfold, and tenfold [2, 3]. Due to this unique structure, QCs have many excellent properties, such as high strength, high electrical resistivity, and wear resistance [2, 4]. For these, more and more attention has been paid to the applications and developments of QCs.

Similar to traditional crystals, piezoelectric quasicrystals (PQCs) possess great application potential in sensors and actuators [5]. However, the piezoelectric effect in QCs is induced by the phonon field or phason field [6], which makes the investigation of PQC more sophisticated, especially for non-homogeneous materials and composite constructions. Therefore, the PQCs have aroused researchers' enormous interest. By virtue of nonlocal strain gradient theory and pseudo-Stroh formalism, Zhang et al. [7] studied functionally graded (FG) one-dimensional (1D) hexagonal PQC multilayered nanoplate, and obtained the exact closed-form expressions of displacements and stresses under multiple loading conditions. Based on the conformal mapping method, Guo and Wang [8] established the three-phase confocal elliptical cylinder model in composite 1D hexagonal PQC, and obtained the solutions of the phonon, phason, and electric fields when the model is subjected to different loading conditions. Mu et al. [9] obtained the generalized uniform/nonuniform stress solutions of critical wedge angles for 1D PQC wedge through the Stroh formalism.

✉ Liangliang Zhang
llzhang@cau.edu.cn

✉ Yang Gao
gaoyangg@gmail.com

1 College of Science, China Agricultural University, Beijing 100083, China

2 College of Engineering, China Agricultural University, Beijing 100083, China

3 Key Laboratory of Microgravity, Institute of Mechanics, Chinese Academy of Sciences, Beijing 100190, China

4 University of Chinese Academy of Sciences, Beijing 100049, China

The problems of PQC composite material with defects (cracks, inclusion, and dislocation) have received considerable attention from investigators. Zhang et al. [10] set the proper potential function and investigated the induction, phonon, and phason stress fields when a spheroidal inclusion was embedded in the matrix of a 1D hexagonal PQC. Zhao et al. [11, 12] analyzed the 3D interface crack of arbitrary shape in 1D hexagonal piezoelectric bi-material QC with thermal effect. Mu et al. [13] discussed the planar problems of FG 2D PQC wedges and spaces with multi-physics loading conditions. Furthermore, with the aid of Stroh formalism, the multi-field coupling problem of an infinite plane containing two dissimilar 1D PQC half-planes was solved by Zhang et al. [14]. These studies contribute to a better understanding of the complex properties of PQC and inspire stress singularity problems.

In engineering applications, composite configurations often contain wedges and junctions. For wedges and junctions, the stress and electric displacement may approach infinity due to discontinuity of geometric and material properties or at sharp corners, which will cause the fracture of structures. Therefore, many researchers have conducted lots of studies on the stress singularities at the wedge apices and junctions for structural safety [15, 16]. Xu and Rajapakse [17] investigated the effects of polarization orientation and electric boundary conditions on the singular orders of piezoelectric composite wedges and junctions by means of extending Lekhnitskii's complex functions. Wang et al. [18] obtained the singular orders of angularly graded piezoelectric composite wedges by the variable separation method. Chen [19] obtained the singular orders by solving the eigen-equation and demonstrated the effects of geometric and material properties on them for multi-material wedges and junctions. Based on the Stroh formalism, Hwu et al. [20–23] presented the analytical solutions for the singular orders of composite wedges and spaces under different boundary conditions. Chuang et al. [24] considered singular orders of a single wedge with mixed boundary conditions and discussed the effect of the alignment of material principal axes on stress singularities.

To the best of the authors' knowledge, the singularities of QC composite wedges and spaces have not been investigated. In this paper, the general anisotropic singularity problem is extended to the more complex 3D cubic PQCs, with the aid of Stroh formalism and Barnett–Lothe matrices. The analytical expressions containing piezoelectric, phonon, and phason constants for the singular orders are firstly established by simple multiplication of the crucial matrix. The singular orders of piezoelectric material are compared with the existing results to verify the accuracy of numerical results. Moreover, the effects of phonon, phason, and electric fields on singularities are discussed in detail. Numerical results show that there exist no singularities when PQC 1—PQC 2/PQC 3 are fully bonded, and the electric field has a weak effect on singularities (see Figs. 4, 6).

2 Stroh Formalism

In this section, we consider 3D cubic PQCs with the symmetry of cubic crystals [2]. They possess quasi-periodic atomic arrangement in each direction (x_1, x_2 and x_3) [25] and polarize in the x_3-axis. According to QC elastic theory [25], the geometric equations of 3D cubic PQCs are expressed as

$$\varepsilon_{ij} = \frac{1}{2}\left(\frac{\partial u_i}{\partial x_j} + \frac{\partial u_j}{\partial x_i}\right), \quad w_{ij} = \frac{1}{2}\left(\frac{\partial w_i}{\partial x_j} + \frac{\partial w_j}{\partial x_i}\right),$$
$$E_i = -\frac{\partial \phi}{\partial x_i} \tag{1}$$

where $i, j = 1, 2, 3$, the phonon displacements u_i denote atomic translation; the phason displacements w_i denote rearrangements of atoms along the quasi-periodic directions [2]; ε_{ij}, w_{ij}, E_i, ϕ represent phonon strains, phason strains, electric field intensities, and electric potential, respectively.

The constitutive equations with point group $\bar{4}3m$ can be written as [6]

$$\begin{aligned}
\sigma_{11} &= C_{11}\varepsilon_{11} + C_{12}\varepsilon_{22} + C_{12}\varepsilon_{33} + R_1 w_{11} + R_2 w_{22} + R_2 w_{33}\\
\sigma_{22} &= C_{12}\varepsilon_{11} + C_{11}\varepsilon_{22} + C_{12}\varepsilon_{33} + R_2 w_{11} + R_1 w_{22} + R_2 w_{33}\\
\sigma_{33} &= C_{12}\varepsilon_{11} + C_{12}\varepsilon_{22} + C_{11}\varepsilon_{33} + R_2 w_{11} + R_2 w_{22} + R_1 w_{33}\\
\sigma_{23} &= \sigma_{32} = 2C_{44}\varepsilon_{23} + 2R_3 w_{23} - d_{14}E_1\\
\sigma_{31} &= \sigma_{13} = 2C_{44}\varepsilon_{31} + 2R_3 w_{31} - d_{14}E_2\\
\sigma_{12} &= \sigma_{21} = 2C_{44}\varepsilon_{12} + 2R_3 w_{12} - d_{14}E_3\\
H_{11} &= R_1\varepsilon_{11} + R_2\varepsilon_{22} + R_2\varepsilon_{33} + K_{11}w_{11} + K_{12}w_{22} + K_{12}w_{33}\\
H_{22} &= R_2\varepsilon_{11} + R_1\varepsilon_{22} + R_2\varepsilon_{33} + K_{12}w_{11} + K_{11}w_{22} + K_{12}w_{33}\\
H_{33} &= R_2\varepsilon_{11} + R_2\varepsilon_{22} + R_1\varepsilon_{33} + K_{12}w_{11} + K_{12}w_{22} + K_{11}w_{33}\\
H_{23} &= H_{32} = 2R_3\varepsilon_{23} + 2K_{44}w_{23} - d_{123}E_1\\
H_{31} &= H_{13} = 2R_3\varepsilon_{31} + 2K_{44}w_{31} - d_{123}E_2\\
H_{12} &= H_{21} = 2R_3\varepsilon_{12} + 2K_{44}w_{12} - d_{123}E_3\\
D_1 &= 2d_{14}\varepsilon_{23} + 2d_{123}w_{23} + \xi_{11}E_1\\
D_2 &= 2d_{14}\varepsilon_{31} + 2d_{123}w_{31} + \xi_{22}E_2\\
D_3 &= 2d_{14}\varepsilon_{12} + 2d_{123}w_{12} + \xi_{33}E_3
\end{aligned} \tag{2}$$

where σ_{ij}, H_{ij} are the stresses in phonon and phason fields, respectively. Phonon stresses σ_{ij} are analogous to crystals, while phason stresses H_{ij} denote the stress components along the x_i-direction in the vertical space $E_\perp^3$ applied on the surface orthogonal to the x_j-direction in the physical space $E_\parallel^3$ [26]. D_j represent electric displacements; C_{ij}, K_{ij} are the elastic constants in phonon and phason fields, respectively;

R_{ij} are the coupling elastic constants; d_{14} and d_{123} are the piezoelectric constants in phonon and phason fields, respectively; and ξ_{ij} are the dielectric constants.

The equilibrium equations without body force are expressed as

$$\partial_j \sigma_{ij} = 0, \quad \partial_j H_{ij} = 0, \quad \partial_j D_j = 0. \tag{3}$$

Considering the 2D deformation problem, the generalized displacements $\boldsymbol{u}$ and stresses $\boldsymbol{\varphi}$ satisfying Eqs. (1), (2), and (3) are assumed to take the following form [14]

$$\boldsymbol{u} = \boldsymbol{a} f(z), \ \boldsymbol{\varphi} = \boldsymbol{b} f(z), \ z = x_1 + p x_3 \tag{4}$$

where f is an arbitrary function of z; $\boldsymbol{a}, \boldsymbol{b}$, and p are constants to be determined by the following eigen-relation

$$\boldsymbol{N} \begin{bmatrix} \boldsymbol{a} \\ \boldsymbol{b} \end{bmatrix} = p \begin{bmatrix} \boldsymbol{a} \\ \boldsymbol{b} \end{bmatrix} \tag{5}$$

$$\boldsymbol{N} = \begin{bmatrix} \boldsymbol{N}_1 & \boldsymbol{N}_2 \\ \boldsymbol{N}_3 & \boldsymbol{N}_1^{\mathrm{T}} \end{bmatrix}, \ \boldsymbol{N}_1 = -\boldsymbol{T}^{-1}\boldsymbol{R}^{\mathrm{T}},$$
$$\boldsymbol{N}_2 = \boldsymbol{T}^{-1}, \ \boldsymbol{N}_3 = \boldsymbol{R}\boldsymbol{T}^{-1}\boldsymbol{R}^{\mathrm{T}} - \boldsymbol{Q} \tag{6}$$

In Eqs. (5) and (6), $p_\alpha (\alpha = 1, 2, \ldots, 7)$, $\boldsymbol{a}_\alpha$ and $\boldsymbol{b}_\alpha$ are, respectively, seven pairs of complex conjugates since strain energy is positive definite. $\boldsymbol{Q}$, $\boldsymbol{R}$, and $\boldsymbol{T}$ are 7×7 real matrices, which can be denoted by Eq. (A1) in the "Appendix." The superscript T denotes matrix transpose.

We have,

$$p_{\alpha+7} = \overline{p}_\alpha, \ \mathrm{Im} p_\alpha > 0 \tag{7}$$

$$\boldsymbol{a}_{\alpha+7} = \overline{\boldsymbol{a}}_\alpha, \ \boldsymbol{b}_{\alpha+7} = \overline{\boldsymbol{b}}_\alpha \tag{8}$$

where Im represents the imaginary part and the overbar denotes the complex conjugate. Once $p_\alpha, \boldsymbol{a}_\alpha$ and $\boldsymbol{b}_\alpha$ are determined, $\boldsymbol{u}$ and $\boldsymbol{\varphi}$ can be represented as

$$\boldsymbol{u} = \boldsymbol{A}\boldsymbol{f}(z_\alpha) + \overline{\boldsymbol{A}\boldsymbol{f}(z_\alpha)}, \ \boldsymbol{\varphi} = \boldsymbol{B}\boldsymbol{f}(z_\alpha) + \overline{\boldsymbol{B}\boldsymbol{f}(z_\alpha)},$$
$$z_\alpha = x_1 + p_\alpha x_3 \tag{9}$$

where

$$\boldsymbol{A} = \{\boldsymbol{a}_1, \boldsymbol{a}_2, \boldsymbol{a}_3, \boldsymbol{a}_4, \boldsymbol{a}_5, \boldsymbol{a}_6, \boldsymbol{a}_7\},$$
$$\boldsymbol{B} = \{\boldsymbol{b}_1, \boldsymbol{b}_2, \boldsymbol{b}_3, \boldsymbol{b}_4, \boldsymbol{b}_5, \boldsymbol{b}_6, \boldsymbol{b}_7\},$$
$$\boldsymbol{f}(z_\alpha) = \Big\{ f_1(z_1), \ f_2(z_2), \ f_3(z_3), \ f_4(z_4), \ f_5(z_5), \ f_6(z_6), \ f_7(z_7) \Big\}^{\mathrm{T}} \tag{10}$$

The Barnett–Lothe matrices $\boldsymbol{S}$, $\boldsymbol{H}$, and $\boldsymbol{L}$ are introduced as

$$\begin{bmatrix} \boldsymbol{A}\boldsymbol{B}^{\mathrm{T}} & \boldsymbol{A}\boldsymbol{A}^{\mathrm{T}} \\ \boldsymbol{B}\boldsymbol{B}^{\mathrm{T}} & \boldsymbol{B}\boldsymbol{A}^{\mathrm{T}} \end{bmatrix} = \frac{1}{2} \begin{bmatrix} \boldsymbol{I} - \mathrm{i}\boldsymbol{S} & -\mathrm{i}\boldsymbol{H} \\ \mathrm{i}\boldsymbol{L} & \boldsymbol{I} - \mathrm{i}\boldsymbol{S}^{\mathrm{T}} \end{bmatrix} \tag{11}$$

$\boldsymbol{A}$ and $\boldsymbol{B}$ have the following orthogonal relation

$$\begin{aligned} \boldsymbol{B}^{\mathrm{T}}\boldsymbol{A} + \boldsymbol{A}^{\mathrm{T}}\boldsymbol{B} &= \boldsymbol{I} = \overline{\boldsymbol{B}}^{\mathrm{T}}\overline{\boldsymbol{A}} + \overline{\boldsymbol{A}}^{\mathrm{T}}\overline{\boldsymbol{B}} \\ \boldsymbol{B}^{\mathrm{T}}\overline{\boldsymbol{A}} + \boldsymbol{A}^{\mathrm{T}}\overline{\boldsymbol{B}} &= \boldsymbol{0} = \overline{\boldsymbol{B}}^{\mathrm{T}}\boldsymbol{A} + \overline{\boldsymbol{A}}^{\mathrm{T}}\boldsymbol{B} \end{aligned} \tag{12}$$

Considering the polar coordinate system (r, θ), Eq. (5) is rewritten as

$$\hat{\boldsymbol{N}}(\theta)\boldsymbol{\xi} = \hat{p}(\theta)\boldsymbol{\xi} \tag{13}$$

where

$$\boldsymbol{\xi} = \{\boldsymbol{a}, \boldsymbol{b}\}^{\mathrm{T}}, \ \hat{\boldsymbol{N}}(\theta) = \cos\theta \boldsymbol{I} + \sin\theta \boldsymbol{N}, \ \hat{p}_\alpha(\theta) = \cos\theta + p_\alpha \sin\theta \tag{14}$$

The surface tractions $\boldsymbol{t}_\theta$ and $\boldsymbol{t}_r$ on the surface $\theta =$ constant and surface $r =$ constant, respectively, are expressed as

$$\boldsymbol{t}_\theta = \boldsymbol{\varphi}_{,r}, \ \boldsymbol{t}_r = -\boldsymbol{\varphi}_{,\theta}/r \tag{15}$$

3 Stress Singularities of Composite Wedges and Spaces

Out of consideration for stress singularities, stress function can be assumed to have the exponential form. Therefore, substituting $< z_\alpha^{1+\delta} > \boldsymbol{g}$ for $\boldsymbol{f}(z_\alpha)$ in Eq. (9), we have

$$\begin{aligned} \boldsymbol{u} &= \boldsymbol{A} < z_\alpha^{1+\delta} > \boldsymbol{g} + \overline{\boldsymbol{A}} < \overline{z}_\alpha^{1+\overline{\delta}} > \overline{\boldsymbol{g}} \\ \boldsymbol{\varphi} &= \boldsymbol{B} < z_\alpha^{1+\delta} > \boldsymbol{g} + \overline{\boldsymbol{B}} < \overline{z}_\alpha^{1+\overline{\delta}} > \overline{\boldsymbol{g}} \end{aligned} \tag{16}$$

where $< >$ denotes diagonal matrix.

If δ is a complex number, they may appear as a pair of complex conjugate to ensure that the displacements and stresses have real values. By superposition of this pair, Eq. (16) can be represented as [27]

$$\begin{aligned} \boldsymbol{u} &= \boldsymbol{A} < z_\alpha^{1+\delta} > \boldsymbol{g} + \overline{\boldsymbol{A}} < \overline{z}_\alpha^{1+\overline{\delta}} > \overline{\boldsymbol{g}} + \boldsymbol{A} < z_\alpha^{1+\overline{\delta}} > \boldsymbol{g}_c \\ &\quad + \overline{\boldsymbol{A}} < \overline{z}_\alpha^{1+\delta} > \overline{\boldsymbol{g}}_c \\ \boldsymbol{\varphi} &= \boldsymbol{B} < z_\alpha^{1+\delta} > \boldsymbol{g} + \overline{\boldsymbol{B}} < \overline{z}_\alpha^{1+\overline{\delta}} > \overline{\boldsymbol{g}} + \boldsymbol{B} < z_\alpha^{1+\overline{\delta}} > \boldsymbol{g}_c \\ &\quad + \overline{\boldsymbol{B}} < \overline{z}_\alpha^{1+\delta} > \overline{\boldsymbol{g}}_c \end{aligned} \tag{17}$$

For the convenience of latter derivation, we have

$$\begin{aligned} \boldsymbol{u} &= \boldsymbol{A} < z_\alpha^{1+\delta} > \boldsymbol{g} + \overline{\boldsymbol{A}} < \overline{z}_\alpha^{1+\delta} > \boldsymbol{h} \\ \boldsymbol{\varphi} &= \boldsymbol{B} < z_\alpha^{1+\delta} > \boldsymbol{g} + \overline{\boldsymbol{B}} < \overline{z}_\alpha^{1+\delta} > \boldsymbol{h} \end{aligned} \tag{18}$$

In the polar coordinate system, with the aid of Eqs. (14) and (15), Eq. (18) is rewritten as

$$\begin{aligned} \boldsymbol{u} &= r^{1+\delta}[\boldsymbol{A} < \hat{p}_\alpha^{1+\delta}(\theta) > \boldsymbol{g} + \overline{\boldsymbol{A}} < \overline{\hat{p}}_\alpha^{1+\delta}(\theta) > \boldsymbol{h}] \\ \boldsymbol{t} &= (1+\delta) r^{\delta}[\boldsymbol{B} < \hat{p}_\alpha^{1+\delta}(\theta) > \boldsymbol{g} + \overline{\boldsymbol{B}} < \overline{\hat{p}}_\alpha^{1+\delta}(\theta) > \boldsymbol{h}] \end{aligned} \tag{19}$$

where θ = constant, $\boldsymbol{g}$ and $\boldsymbol{h}$ are two complex coefficient vectors which are determined by boundary conditions.

Williams [28] assumed that the stresses near the apex are proportional to r^{δ}. If $\mathrm{Re}(\delta) < 0$, the stress is singular at the wedge apex $r = 0$. When $\mathrm{Re}(\delta) < -1$, the strain energy of the elastic wedge may become unbounded. So, we are interested in the region where the real part of δ is in the range

$$-1 < \mathrm{Re}(\delta) < 0 \tag{20}$$

The purpose of this paper is to investigate the appearance of any value of δ which lies in this region. The singular orders are governed by $\mathrm{Re}(\delta)$. Moreover, the existence of a non-vanishing imaginary part of δ leads to oscillatory singularity [29].

Using Eq. (14), Eq. (18) is written in matrix form

$$\begin{bmatrix} \boldsymbol{u} \\ \boldsymbol{\varphi} \end{bmatrix} = r^{1+\delta} \begin{bmatrix} \boldsymbol{A} & \overline{\boldsymbol{A}} \\ \boldsymbol{B} & \overline{\boldsymbol{B}} \end{bmatrix} \begin{bmatrix} < \hat{p}_\alpha^{1+\delta}(\theta) > & \boldsymbol{0} \\ \boldsymbol{0} & < \overline{\hat{p}}_\alpha^{1+\delta}(\theta) > \end{bmatrix} \begin{bmatrix} \boldsymbol{g} \\ \boldsymbol{h} \end{bmatrix} \tag{21}$$

We have [30]

$$\hat{\boldsymbol{N}}(\theta) = \begin{bmatrix} \boldsymbol{A} & \overline{\boldsymbol{A}} \\ \boldsymbol{B} & \overline{\boldsymbol{B}} \end{bmatrix} \begin{bmatrix} < \hat{p}_\alpha(\theta) > & \boldsymbol{0} \\ \boldsymbol{0} & < \overline{\hat{p}}_\alpha(\theta) > \end{bmatrix} \begin{bmatrix} \boldsymbol{B}^{\mathrm{T}} & \boldsymbol{A}^{\mathrm{T}} \\ \overline{\boldsymbol{B}}^{\mathrm{T}} & \overline{\boldsymbol{A}}^{\mathrm{T}} \end{bmatrix} \tag{22}$$

$$\hat{p}(\theta)\hat{p}^{-1}(\theta_0) = \hat{p}(\theta, \theta_0), \ \ \hat{\boldsymbol{N}}(\theta, \omega)\hat{\boldsymbol{N}}(\omega, \theta_0) = \hat{\boldsymbol{N}}(\theta, \theta_0) \tag{23}$$

$$\hat{\boldsymbol{N}}(\theta)\hat{\boldsymbol{N}}^{-1}(\theta_0) = \hat{\boldsymbol{N}}(\theta, \theta_0), \ \ \hat{\boldsymbol{N}}^{\lambda}(\theta, \theta_0)\hat{\boldsymbol{N}}^{\lambda}(\theta_0, \theta) = \boldsymbol{I} \tag{24}$$

Using Eqs. (22), (23), (24), and (12), one has

$$\hat{\boldsymbol{N}}^{1+\delta}(\theta, \omega) = \begin{bmatrix} \boldsymbol{A} & \overline{\boldsymbol{A}} \\ \boldsymbol{B} & \overline{\boldsymbol{B}} \end{bmatrix} \begin{bmatrix} < \hat{p}_\alpha^{1+\delta}(\theta, \omega) > & \boldsymbol{0} \\ \boldsymbol{0} & < \overline{\hat{p}}_\alpha^{1+\delta}(\theta, \omega) > \end{bmatrix} \begin{bmatrix} \boldsymbol{B}^{\mathrm{T}} & \boldsymbol{A}^{\mathrm{T}} \\ \overline{\boldsymbol{B}}^{\mathrm{T}} & \overline{\boldsymbol{A}}^{\mathrm{T}} \end{bmatrix} \tag{25}$$

$$\hat{\boldsymbol{N}}^{\lambda}(\omega, \beta) = \begin{bmatrix} \boldsymbol{A} & \overline{\boldsymbol{A}} \\ \boldsymbol{B} & \overline{\boldsymbol{B}} \end{bmatrix} \begin{bmatrix} < \hat{p}_\alpha^{\lambda}(\omega)\hat{p}_\alpha^{-\lambda}(\beta) > & \boldsymbol{0} \\ \boldsymbol{0} & < \overline{\hat{p}}_\alpha^{\lambda}(\omega)\overline{\hat{p}}_\alpha^{-\lambda}(\beta) > \end{bmatrix} \begin{bmatrix} \boldsymbol{B}^{\mathrm{T}} & \boldsymbol{A}^{\mathrm{T}} \\ \overline{\boldsymbol{B}}^{\mathrm{T}} & \overline{\boldsymbol{A}}^{\mathrm{T}} \end{bmatrix} \tag{26}$$

$\hat{\boldsymbol{N}}^{\lambda}(\omega, \beta)$ plays an important role in determining the singularities.

3.1 Composite Spaces

Considering an infinite composite space ($\theta_n = \theta_0 + 2\pi$) that contains several wedges, the nth wedge is fully bonded to the first wedge, as shown in Fig. 1.

Assuming that n dissimilar wedges are perfectly connected at the interface, each wedge is located in the following region

$$\theta_{k-1} \le \theta \le \theta_k, \quad k = 1, 2, \ldots, n \tag{27}$$

Displacement continuity at each interface is

$$\boldsymbol{u}_k(\theta_k) = \boldsymbol{u}_{k+1}(\theta_k), \quad \boldsymbol{u}_n(\theta_n) = \boldsymbol{u}_1(\theta_0), \quad k = 1, 2, \ldots, n-1 \tag{28}$$

From Eq. (15), we know that the traction continuity conditions can be replaced by stress function continuity, so we have

$$\boldsymbol{\varphi}_k(\theta_k) = \boldsymbol{\varphi}_{k+1}(\theta_k), \quad \boldsymbol{\varphi}_n(\theta_n) = \boldsymbol{\varphi}_1(\theta_0) \tag{29}$$

where the subscript k denotes the kth wedge.

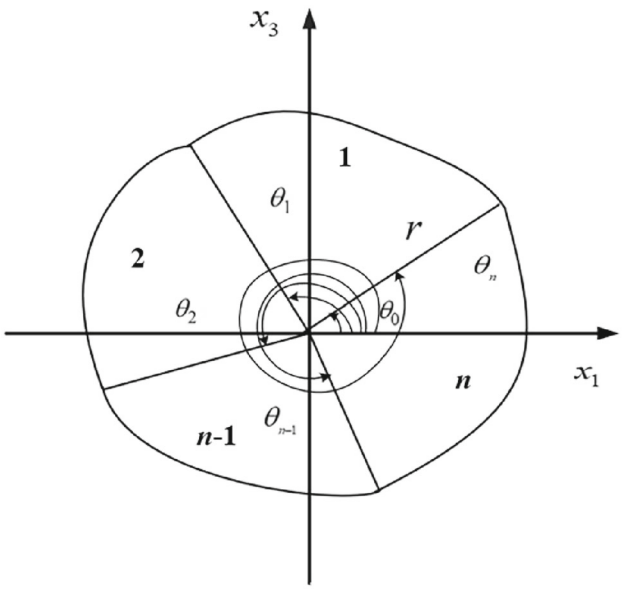

Fig. 1 The 3D cubic PQC composite space

Letting Eqs. (28)$_1$ and (29)$_1$ equal to $\boldsymbol{p}_k$ and $\boldsymbol{q}_k$, respectively, with the aid of Eq. (21), we obtain

$$\begin{bmatrix} \boldsymbol{p}_k \\ \boldsymbol{q}_k \end{bmatrix} = \hat{\boldsymbol{N}}_{k+1}^{1+\delta}(\theta_k, \theta_{k+1}) \begin{bmatrix} \boldsymbol{p}_{k+1} \\ \boldsymbol{q}_{k+1} \end{bmatrix} \tag{30}$$

where $\boldsymbol{p}_k$ and $\boldsymbol{q}_k$ are 7×1 vectors, $\hat{\boldsymbol{N}}_{k+1}^{1+\delta}(\theta_k, \theta_{k+1})$ is the crucial matrix containing singular orders. The derivation process of Eq. (30) is shown in Eqs. (A2)–(A4) in the "Appendix."

In Eq. (A3), setting $k = 1$ for $(\boldsymbol{g}_k, \boldsymbol{h}_k)$ and $k = n - 1$ for $(\boldsymbol{g}_{k+1}, \boldsymbol{h}_{k+1})$ to get two new equations and substituting them into the second equation of Eqs. (28), (29), and (21), we obtain

$$\hat{\boldsymbol{N}}_n^{1+\delta}(\theta_0, \theta_{n-1}) \begin{bmatrix} \boldsymbol{p}_{n-1} \\ \boldsymbol{q}_{n-1} \end{bmatrix} = \hat{\boldsymbol{N}}_1^{1+\delta}(\theta_0, \theta_1) \begin{bmatrix} \boldsymbol{p}_1 \\ \boldsymbol{q}_1 \end{bmatrix} \tag{31}$$

By using Eq. (31) and repeatedly using Eq. (30), one has

$$\left[\hat{\boldsymbol{N}}_n^{1+\delta}(\theta_0, \theta_{n-1}) - \prod_{j=1}^{n-1} \hat{\boldsymbol{N}}_j^{1+\delta}(\theta_{j-1}, \theta_j) \right] \begin{bmatrix} \boldsymbol{p}_{n-1} \\ \boldsymbol{q}_{n-1} \end{bmatrix} = \boldsymbol{0} \tag{32}$$

We assume that

$$\begin{bmatrix} \boldsymbol{p}_{n-1} \\ \boldsymbol{q}_{n-1} \end{bmatrix} = \hat{\boldsymbol{N}}_n^{1+\delta}(\theta_{n-1}, \theta_n) \begin{bmatrix} \boldsymbol{p}_* \\ \boldsymbol{q}_* \end{bmatrix} \tag{33}$$

where $\boldsymbol{p}_*$ and $\boldsymbol{q}_*$ are unknown vectors.

Substituting Eq. (33) into Eq. (32), and using Eq. (24), we have

$$[\boldsymbol{E} - \boldsymbol{I}] \begin{bmatrix} \boldsymbol{p}_* \\ \boldsymbol{q}_* \end{bmatrix} = \boldsymbol{0} \tag{34}$$

Nontribal solutions for Eq. (34) exist, if

$$\det(\boldsymbol{E} - \boldsymbol{I}) = 0 \tag{35}$$

where

$$\boldsymbol{E} = \prod_{j=1}^{n} \hat{\boldsymbol{N}}_j^{1+\delta}(\theta_{j-1}, \theta_j) \tag{36}$$

The values of δ can be determined by Eqs. (35) and (36).

3.2 Composite Wedges

In this section, considering a composite wedge ($\theta_n < \theta_0 + 2\pi$) composed of several wedges, where the (k-1)th wedge is bonded together with the kth ($k = 2,3,\ldots,n$) wedge, we have the following four types of boundary conditions

$$\begin{aligned} &\boldsymbol{\varphi}_1(\theta_0) = \boldsymbol{0}, \quad \boldsymbol{u}_n(\theta_n) = \boldsymbol{0} \\ &\boldsymbol{u}_k(\theta_k) = \boldsymbol{u}_{k+1}(\theta_k), \quad \boldsymbol{\varphi}_k(\theta_k) = \boldsymbol{\varphi}_{k+1}(\theta_k) \\ &\quad k = 1, 2, \ldots, n-1 \end{aligned} \tag{37}$$

$$\begin{aligned} &\boldsymbol{u}_1(\theta_0) = \boldsymbol{0}, \quad \boldsymbol{u}_n(\theta_n) = \boldsymbol{0} \\ &\boldsymbol{u}_k(\theta_k) = \boldsymbol{u}_{k+1}(\theta_k), \quad \boldsymbol{\varphi}_k(\theta_k) = \boldsymbol{\varphi}_{k+1}(\theta_k) \end{aligned} \tag{38}$$

$$\begin{aligned} &\boldsymbol{\varphi}_1(\theta_0) = \boldsymbol{0}, \quad \boldsymbol{\varphi}_n(\theta_n) = \boldsymbol{0} \\ &\boldsymbol{u}_k(\theta_k) = \boldsymbol{u}_{k+1}(\theta_k), \quad \boldsymbol{\varphi}_k(\theta_k) = \boldsymbol{\varphi}_{k+1}(\theta_k) \end{aligned} \tag{39}$$

$$\begin{aligned} &\boldsymbol{u}_1(\theta_0) = \boldsymbol{0}, \quad \boldsymbol{\varphi}_n(\theta_n) = \boldsymbol{0} \\ &\boldsymbol{u}_k(\theta_k) = \boldsymbol{u}_{k+1}(\theta_k), \quad \boldsymbol{\varphi}_k(\theta_k) = \boldsymbol{\varphi}_{k+1}(\theta_k) \end{aligned} \tag{40}$$

Equations (37)–(40) are called the free–fixed, fixed—fixed, free–free, and fixed–free ("free" means traction-free and electrically open, and "fixed" means clamped and electrically closed) wedges, respectively. Since the continuity conditions in Eqs. (37)–(40) are the same as those in Eqs. (28)$_1$ and (29)$_1$, we may use the results of Eqs. (30), (33), and (36) in the subsequent calculation.

Free–Fixed Composite Wedge. Using Eqs. (30) and (37), we obtain

$$\begin{bmatrix} \hat{\boldsymbol{N}}_{1L}^{1+\delta}(\theta_0, \theta_1) \prod_{j=2}^{n-1} \hat{\boldsymbol{N}}_j^{1+\delta}(\theta_{j-1}, \theta_j) \\ \hat{\boldsymbol{N}}_{nU}^{1+\delta}(\theta_n, \theta_{n-1}) \end{bmatrix} \begin{bmatrix} \boldsymbol{p}_{n-1} \\ \boldsymbol{q}_{n-1} \end{bmatrix} = \boldsymbol{0} \tag{41}$$

where the subscripts L and U represent the lower half part of the matrix and the upper half part of the matrix, respectively. For example, $\boldsymbol{\xi}_U = \boldsymbol{a}$ for Eq. (14). The derivation process of Eq. (41) is shown in Eq. (A5)–(A6) in Appendix.

Substituting Eq. (33) into Eq. (41) and using Eq. (24), we have

$$\hat{\boldsymbol{N}}_{1L}^{1+\delta}(\theta_0, \theta_1) \prod_{j=2}^{n} \hat{\boldsymbol{N}}_j^{1+\delta}(\theta_{j-1}, \theta_j) \begin{bmatrix} \boldsymbol{p}_* \\ \boldsymbol{q}_* \end{bmatrix} = \boldsymbol{0} \tag{42}$$

$$\begin{bmatrix} \boldsymbol{0} & \boldsymbol{I} \end{bmatrix} \begin{bmatrix} \boldsymbol{p}_* \\ \boldsymbol{q}_* \end{bmatrix} = \boldsymbol{0} \tag{43}$$

From Eqs. (42) and (43), we know that

$$\boldsymbol{p}_* = \boldsymbol{0}, \quad \boldsymbol{E}_4 \boldsymbol{q}_* = \boldsymbol{0} \tag{44}$$

where $\boldsymbol{E}_4$ means the lower right of $\boldsymbol{E}$ [Eq. (36)] defined by

$$\boldsymbol{E} = \begin{bmatrix} \boldsymbol{E}_1 & \boldsymbol{E}_2 \\ \boldsymbol{E}_3 & \boldsymbol{E}_4 \end{bmatrix} \tag{45}$$

only when

$$\det(\boldsymbol{E}_4) = 0 \tag{46}$$

the singular orders of the free–fixed composite wedge can be acquired.

Following the same manipulation as the free–fixed wedge, we can get the singular orders for

Fixed–Fixed Wedge,

$$\det(\boldsymbol{E}_2) = 0 \tag{47}$$

Free–Free Wedge,

$$\det(\boldsymbol{E}_3) = 0 \tag{48}$$

Fixed–Free Wedge,

$$\det(\boldsymbol{E}_1) = 0 \tag{49}$$

More importantly, through proper arrangement, the constitutive law, strain–displacement relation, and equilibrium equation of 1D and 2D QCs can be written in the similar mathematical form of 3D cubic QC, and hence the method and formulation here can be extended to other types of QCs.

4 Special Cases of Crack Included

For a semi-infinite crack $(-\pi, \pi)$ in a wedge with fixed–fixed surfaces, Eq. (36) may become

$$\begin{aligned}\det(&\boldsymbol{A} < \hat{p}_\alpha^{1+\delta}(\theta_0)\hat{p}_\alpha^{-1-\delta}(\theta_1) > \boldsymbol{A}^{\mathrm{T}} \\ &+ \overline{\boldsymbol{A}} < \overline{\hat{p}}_\alpha^{1+\delta}(\theta_0)\overline{\hat{p}}_\alpha^{-1-\delta}(\theta_1) > \overline{\boldsymbol{A}}^{\mathrm{T}}) = 0\end{aligned} \tag{50}$$

With this special angle, Eq. $(14)_3$ may be expressed as

$$\hat{p}_\alpha(\pm\pi) = \mathrm{e}^{\pm \mathrm{i}\pi} \tag{51}$$

Substituting Eq. (51) into Eq. (50) yields

$$|2\sin 2\delta\pi \boldsymbol{H}| = 0 \tag{52}$$

therefore, we have

$$\delta = -0.5 \tag{53}$$

Based on Eq. (52), the singularity has no concern with material constants. The singular orders of a single wedge with free–free, free–fixed, and fixed–free surfaces can be easily obtained by similar operation. Moreover, for anisotropic elastic materials, the singularities of the semi-infinite crack in a single wedge or interfacial crack under different boundary conditions have been investigated by Hwu [20] and Ting [30].

5 Numerical Examples and Discussion

Owing to the difficulty of the experiment, the material constants of cubic QCs of point group $\bar{4}3m$ have not been fully obtained. According to QC elastic theory, the material constants of 3D cubic PQC can be assumed (Table 1).

5.1 The Singularities of a Single Wedge

To verify the correctness of the numerical results, the singular orders are compared between Ref. [17] and our results by considering the PZT-4 wedge with traction-free. Referring to Fig. 2, most of the results are in good agreement with Ref. [17].

For a 3D cubic PQC wedge with a wedge angle 2α, two sides of the wedge are traction-free. Figure 3 shows the variations of singular orders with wedge angles 2α. δ_{ci} $(i = 1,2\ldots)$, δ_{pi} $(i = 1,2\ldots)$, and δ_{ei} $(i = 1,2\ldots)$ denote the ith root produced by the phonon field, phason field, and electric field, respectively. There is no singularity for an infinite half-plane $(2\alpha = 180^\circ)$, but the semi-infinite crack $(2\alpha = 360^\circ)$ shows the strongest singularity. All roots δ are real and four roots exist for all wedge angles, between 180° and 360°. Only one root δ_{e1} is caused by the electric field, which indicates that the electric field has a weak effect on singularities. What's more, the singularities increase as the wedge angle increases.

The singular orders of a single wedge with different boundary conditions are shown in Table 2. There are no singularities for an infinite quarter plane (90°) or half-plane (180°) when two sides of the wedge are free–free and fixed–fixed, respectively. The wedge whose two sides are fixed–fixed produces no singularities except at $2\alpha = 360°$, while the wedge with mixed boundary conditions has singularities between 90° and 360°. By comparing the third column and the sixth column, it is found that if δ is a singular order of an infinite half-plane, then $\delta/2$, $(\delta - 1)/2$ are singular orders of the infinite plane containing semi-infinite crack with identical boundary conditions. Table 2 shows that singular orders have a strong dependence on boundary conditions.

5.2 The Singularities of Bi-material Wedges

Considering a 3D cubic PQC bi-material wedge composed of two dissimilar wedges, it has a debonded interface, and two sides of it are traction-free. The changes of singular orders with wedge angles α are shown in Fig. 4. By comparing the symmetry and the magnitude of the graph, the

Table 1 Material constants of the 3D cubic PQC

Material constants	PQC 1	PQC 2	PQC 3
Phonon field (GPa)	$C_{11} = 166, C_{12} = 77,$ $C_{44} = 88,$	$C_{11} = 286, C_{12} = 173,$ $C_{44} = 170.5,$	$C_{11} = 276, C_{12} = 153,$ $C_{44} = 140.5,$
Phason field (GPa)	$K_{11} = 24,\ K_{12} = 14,$ $K_{44} = 19$	$K_{11} = 145,\ K_{12} = 57,$ $K_{44} = 33$	$K_{11} = 140,\ K_{12} = 55,$ $K_{44} = 31$
Couple field (GPa)	$R_1 = 8.85,$ $R_2 = 4.85,$ $R_3 = 5.85,$	$R_1 = 13.7,\ R_2 = 7.5,$ $R_3 = 10.4,$	$R_1 = 10.7,\ R_2 = 6.5,$ $R_3 = 8.4,$
Piezoelectric Constants (cm^{-2})	$d_{14} = -0.138, d_{123} = -0.16,$	$d_{14} = -0.247, d_{123} = -0.2674,$	$d_{14} = -0.26, d_{123} = -0.287,$
Dielectric Constants ($10^{-9}C^2/(Nm^2)$)	$k_1 = 11.2,\ k_2 = 8.2,$ $k_3 = 4.2.$	$k_1 = 22.4,\ k_2 = 14.3,$ $k_3 = 6.9.$	$k_1 = 21.4,\ k_2 = 11.3,$ $k_3 = 6.9.$

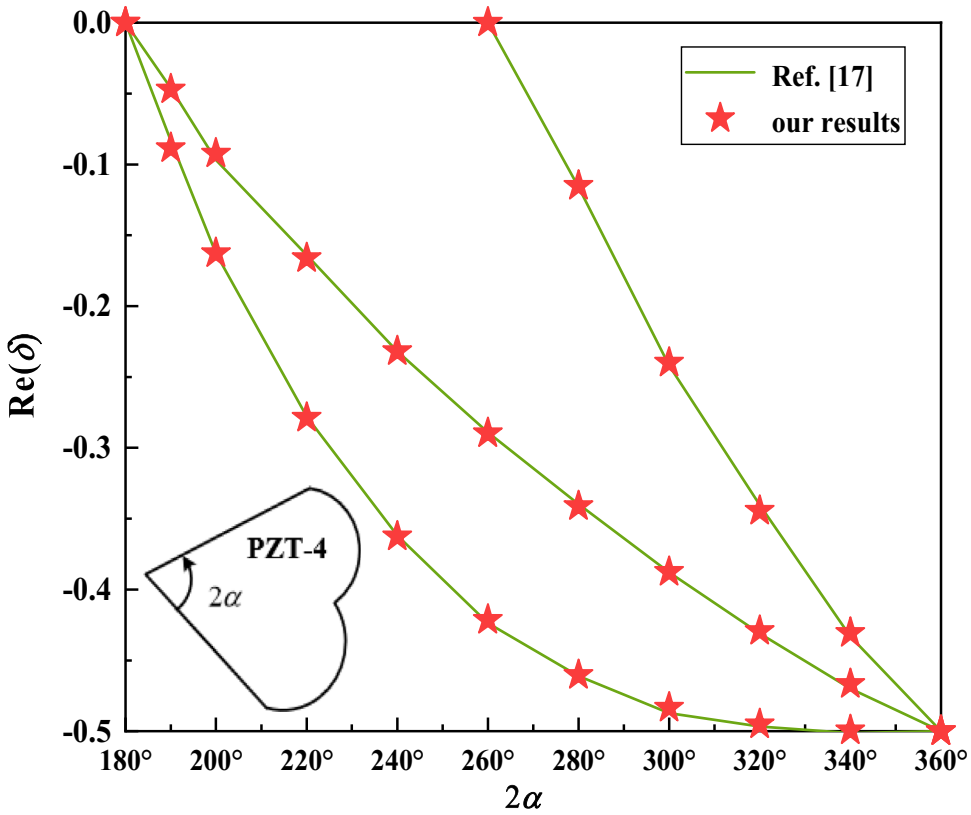

Fig. 2 The comparison of singular orders for PZT-4 wedge

singularities are identical for α and 360°–α showing symmetry about $\alpha = 180°$, and the most critical singular order (−0.54498) produced by the phonon field exists at around 120° (240°). There are no singularities produced by the electric field. Two roots are caused by the phonon field between 90° and 135°, and 225° and 270°, implying that the phonon field has a strong influence on the singularities. Moreover, no singularities occur when PQC 1 and PQC 2 are fully bonded together.

For a 3D cubic PQC bi-material wedge with free–free boundary conditions, the variations of singular orders with wedge angle α are displayed in Fig. 5. Obviously, the singularities show symmetry about $\alpha = 180°$. Two roots caused by the phonon field appear for all wedge angles, between 90° and 270°, and two roots caused by the phason field appear at about 135° and 225°. The singularities induced by the electric field exist between 120° and 150°, and 210° and 240°. Moreover, the strongest singularity (−0.57862) produced by the phonon field exists at around 135° and 225°. Comparison between Figs. 4 and 5 shows that material properties have a great influence on singularities. More importantly, there are

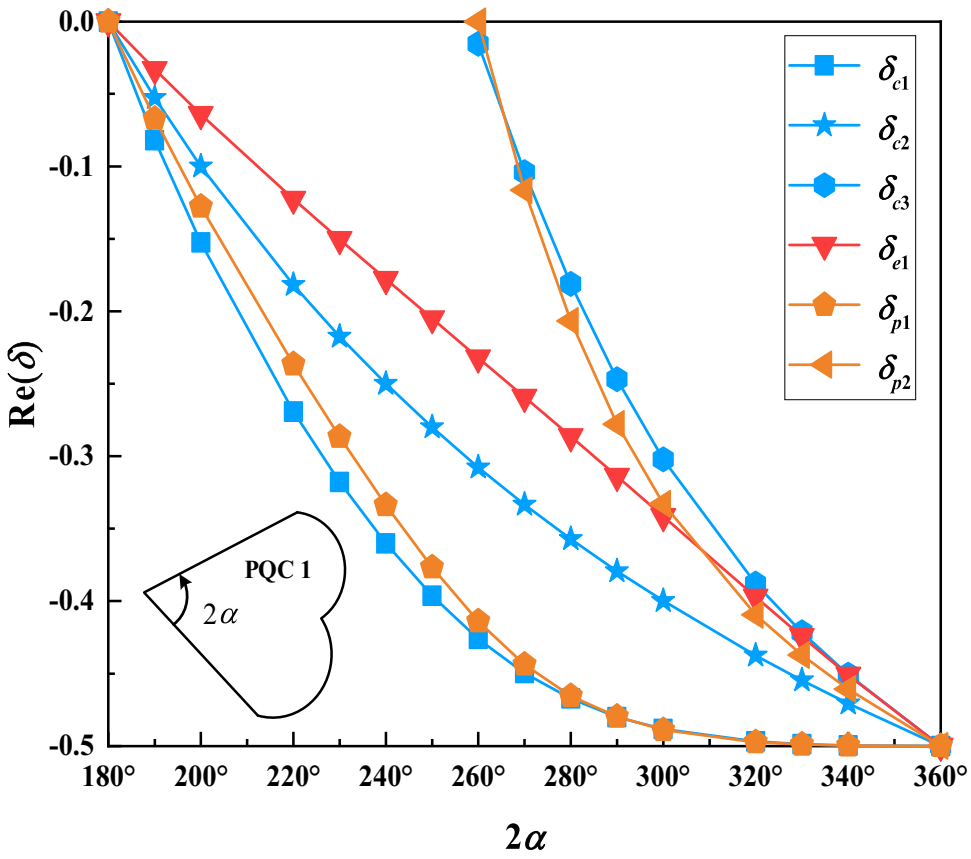

Fig. 3 The singular orders of a 3D cubic PQC wedge with free–free boundary conditions

Table 2 Singular orders for a 3D cubic PQC with different boundary conditions

Boundary conditions	Wedge angles (2α)				
	90°	180°	240°	300°	360°
Free–free	–	–	−0.3602, − 0.25 − 0.1779, − 0. 3337	− 0.4882, − 0.3999 − 0.3022, − 0.3416 −0.4890, −0.3329	− 0.5
Fixed–fixed	–	–	–	–	−0.5
Free–fixed	− 0.2310 − 0.1742	− 0.5013 − 0.5 − 0.4987	− 0.6250, − 0.627, −0.5889	−0.7, − 0.6708 − 0.1422, − 0.1 − 0.0783, − 0.0123	− 0.75 − 0.25

no singularities in the infinite composite space when PQC 1 and PQC 3 are perfectly bonded together.

5.3 The Singularities of Tri-material Wedges

A PQC 1 half-plane and PQC 2 are bonded to PQC 3 under free–free boundary conditions, displayed in Fig. 6. The singular orders induced by the electric field only exist between 180° and 220°, indicating that the electric field has a weak effect on singularities. Two roots are caused by the phason field between 270° and 360°. Moreover, there are no singularities when $\alpha = 180°$, and the strongest singularities appear at $\alpha = 360°$.

The singular orders of a 3D cubic PQC composite wedge with free–fixed boundary conditions are shown in Fig. 7. Only one root is produced by the phason field from 140° to 240°. Three roots are induced by the phonon field: δ_{c1} exists for all wedge angles, indicating that singularities have a strong dependence on the phonon field; but δ_{c2} only occurs between 190° and 230°, and δ_{c3} appears between 190° and 200°. It is worth mentioning that the singularities become more rigorous and then relieve with the increase in α, and the

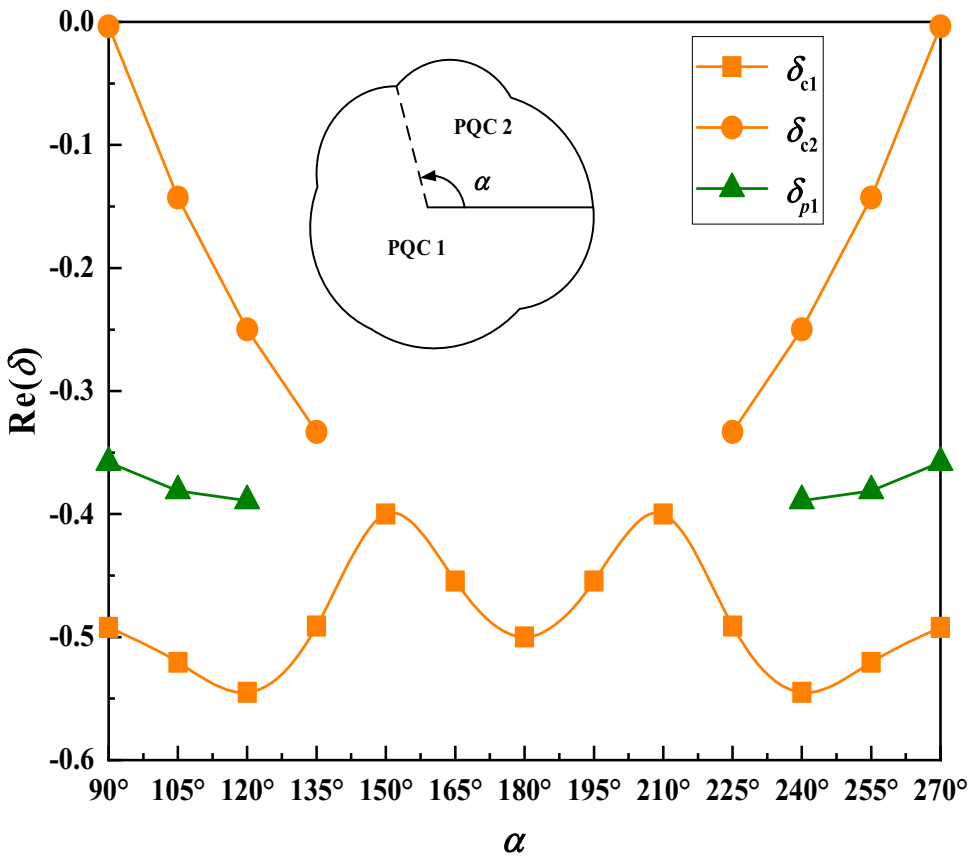

Fig. 4 The singular orders of PQC 1 bonded to PQC 2 with free–free boundary conditions

most critical singular order (-0.6156) caused by the electric field is observed at around 180°.

6 Conclusion

In this paper, the singularities of 3D cubic PQC composite wedges and spaces, for the first time, are explored. Based on the Stroh formalism and the Barnett–Lothe matrices, the crucial matrix determining the singular orders is obtained. Some numerical examples are presented to investigate the effects of phonon, phason, and electric fields on singularities under different boundary conditions. All roots are shown in the numerical study to present a complete picture of the nature of singularities in composite wedges and spaces. The following conclusions can be drawn:

1. If δ is a singular order of an infinite half-plane, then $\delta/2$, $(\delta - 1)/2$ are singular orders for a semi-infinite crack with identical boundary conditions.
2. Quite serious singularities exist in composite wedges and spaces, which are composed of two or three dissimilar material wedges due to the existence of crack or a debonding interface.
3. For tri-material wedges, the singularities may get severe and then relieve with the increase in wedge angle under mixed boundary conditions (see Fig. 7).
4. Fully bonded PQC 1—PQC 2/ PQC 3 do not show any singularities. In some cases, the electric field has a weak effect on singularities (see Figs. 4, 6).

The numerical results are beneficial to performing accurate analysis of stress singularities by considering all roots, provide some theoretical guidance and reference for designing and selecting wedge structures, and more importantly, offer a theoretical reference for material reliability evaluation in engineering applications.

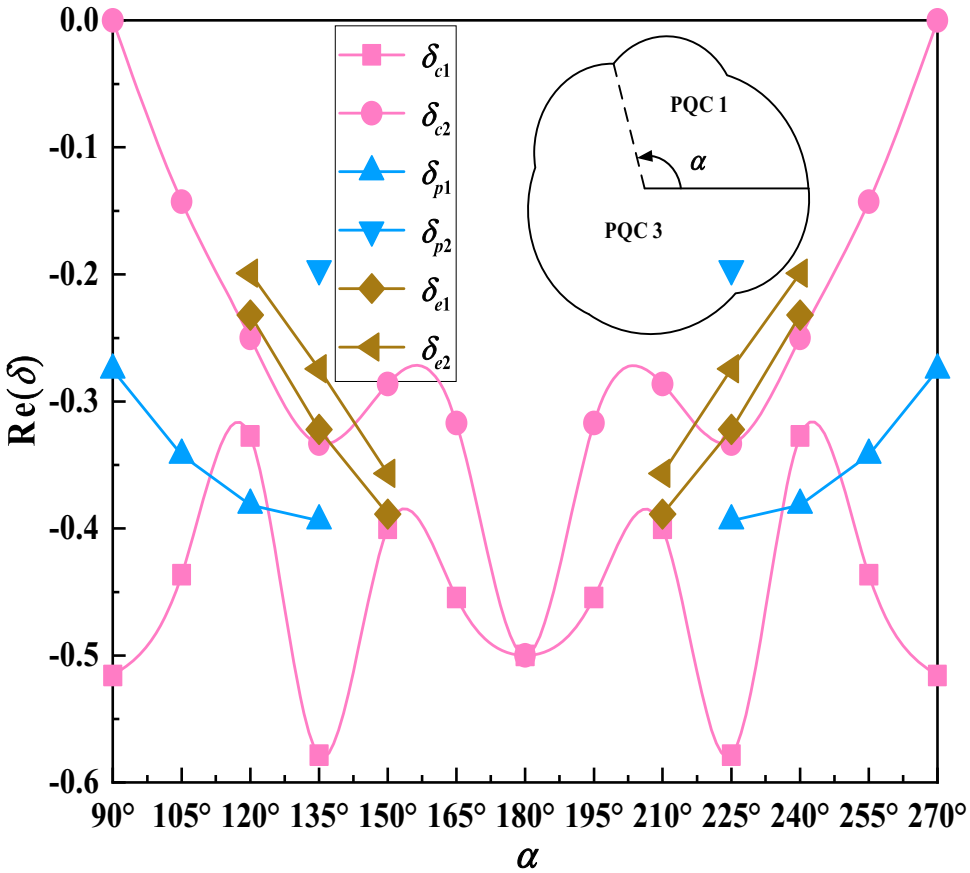

Fig. 5 The singular orders of PQC 1 bonded to PQC 3 with free–free boundary conditions

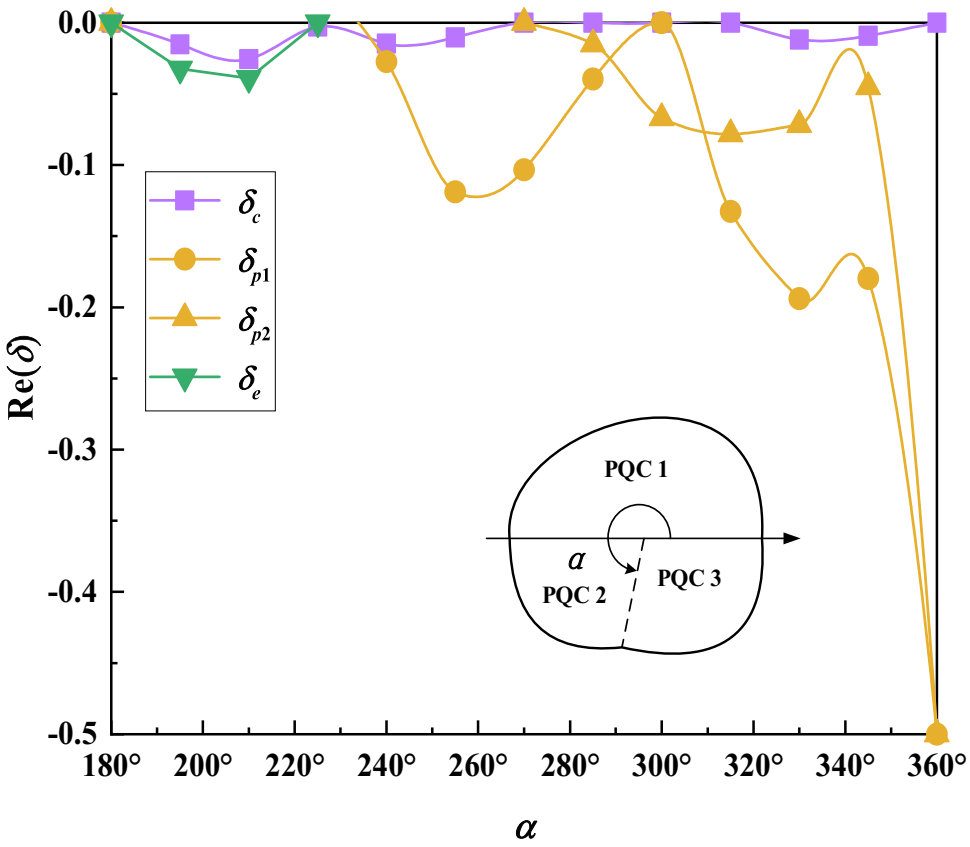

Fig. 6 The singular orders of tri-material wedges under free–free boundary conditions

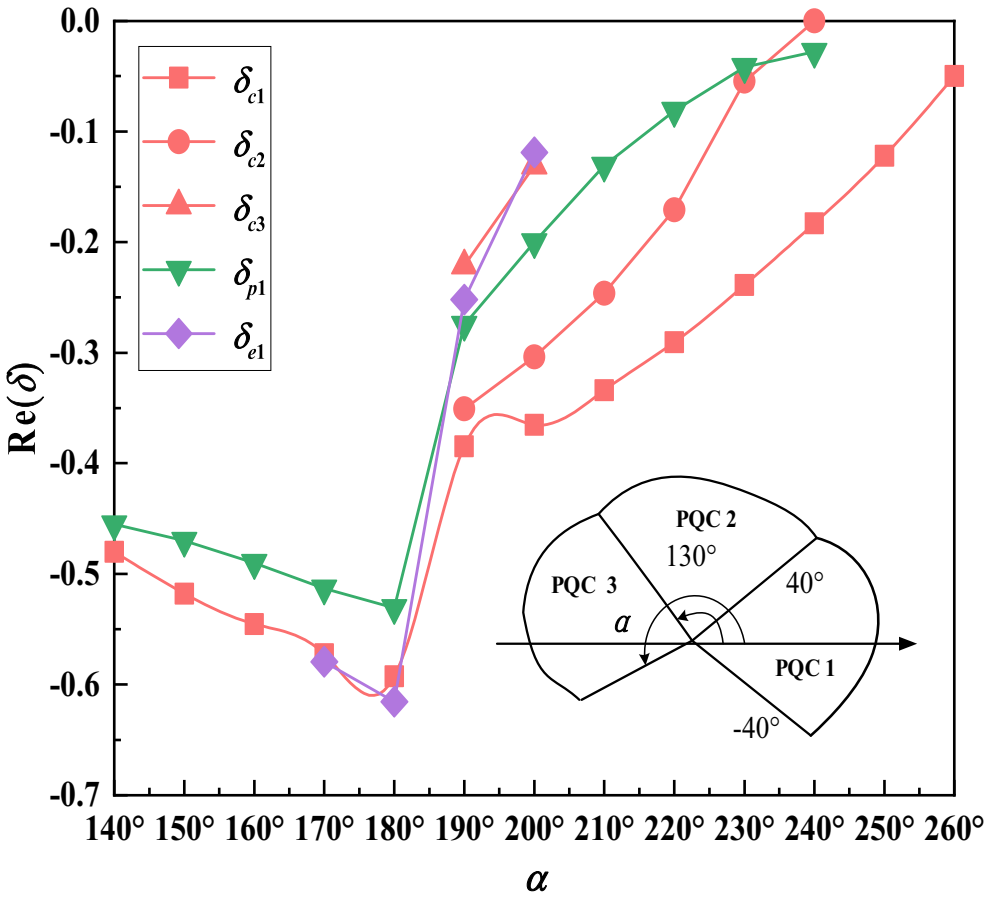

Fig. 7 The singular orders of tri-material wedges with free–fixed boundary conditions

Acknowledgements The authors thank Xiaoyu Fu for helpful discussion.

Author Contributions XM, YG, and LZ conceived the concept and model. XM, TC, and WX carried out the theoretical analyses and numerical simulations. ZZ, TQ, and YG supervised the research. All authors discussed the results and wrote the manuscript.

Funding This work was supported by the National Natural Science Foundation of China (Grant Nos. 11972365 and 12102458) and China Agricultural University Education Foundation (No. 1101-2412001).

Data Availability The data generated or analyzed used to support the findings of this study are included within the article.

Declarations

Conflict of interest No support, financial or otherwise, has been received from any organization that may have an interest in the submitted work; there are no other relationships or activities that could appear to have influenced the submitted work.

Appendix

By using Eqs. (1), (2), (3), and (4), we can obtain the matrics about $x1 - x2$

$$\boldsymbol{Q} = \begin{bmatrix} C_{11} & 0 & 0 & R_1 & 0 & 0 & 0 \\ 0 & C_{44} & 0 & 0 & R_3 & 0 & 0 \\ 0 & 0 & C_{44} & 0 & 0 & R_3 & 0 \\ R_1 & 0 & 0 & K_{11} & 0 & 0 & 0 \\ 0 & R_3 & 0 & 0 & K_{44} & 0 & 0 \\ 0 & 0 & R_3 & 0 & 0 & K_{44} & 0 \\ 0 & 0 & 0 & 0 & 0 & 0 & -\xi_{11} \end{bmatrix},$$

$$\boldsymbol{R} = \begin{bmatrix} 0 & C_{12} & 0 & 0 & R_2 & 0 & 0 \\ C_{44} & 0 & 0 & R_3 & 0 & 0 & 0 \\ 0 & 0 & 0 & 0 & 0 & 0 & d_{14} \\ 0 & R_2 & 0 & 0 & K_{12} & 0 & 0 \\ R_3 & 0 & 0 & K_{44} & 0 & 0 & 0 \\ 0 & 0 & 0 & 0 & 0 & 0 & d_{123} \\ 0 & 0 & d_{14} & 0 & 0 & d_{123} & 0 \end{bmatrix},$$

$$\boldsymbol{T}=\begin{bmatrix} C_{44} & 0 & 0 & R_3 & 0 & 0 & 0 \\ 0 & C_{11} & 0 & 0 & R_1 & 0 & 0 \\ 0 & 0 & C_{44} & 0 & 0 & R_3 & 0 \\ R_3 & 0 & 0 & K_{44} & 0 & 0 & 0 \\ 0 & R_1 & 0 & 0 & K_{11} & 0 & 0 \\ 0 & 0 & R_3 & 0 & 0 & K_{44} & 0 \\ 0 & 0 & 0 & 0 & 0 & 0 & -\xi_{22} \end{bmatrix} \tag{A1}$$

Equations $(28)_1$ and $(29)_1$ are equal to $\boldsymbol{p}_k$ and $\boldsymbol{q}_k$, respectively. With the aid of Eq. (21), we derive

$$\begin{aligned} &\begin{bmatrix} \boldsymbol{A}_k & \bar{\boldsymbol{A}}_k \\ \boldsymbol{B}_k & \bar{\boldsymbol{B}}_k \end{bmatrix}\begin{bmatrix} < \hat{p}_{\alpha k}^{1+\delta}(\theta_k) > & \boldsymbol{0} \\ \boldsymbol{0} & < \bar{\hat{p}}_{\alpha k}^{1+\delta}(\theta_k) > \end{bmatrix}\begin{bmatrix} \boldsymbol{g}_k \\ \boldsymbol{h}_k \end{bmatrix} \\ &= \begin{bmatrix} \boldsymbol{A}_{k+1} & \bar{\boldsymbol{A}}_{k+1} \\ \boldsymbol{B}_{k+1} & \bar{\boldsymbol{B}}_{k+1} \end{bmatrix}\begin{bmatrix} < \hat{p}_{\alpha k+1}^{1+\delta}(\theta_k) > & \boldsymbol{0} \\ \boldsymbol{0} & < \bar{\hat{p}}_{\alpha k+1}^{1+\delta}(\theta_k) > \end{bmatrix}\begin{bmatrix} \boldsymbol{g}_{k+1} \\ \boldsymbol{h}_{k+1} \end{bmatrix} \\ &= \begin{bmatrix} \boldsymbol{p}_k \\ \boldsymbol{q}_k \end{bmatrix} \end{aligned} \tag{A2}$$

Using Eq. (12), $(\boldsymbol{g}_k, \boldsymbol{h}_k)$ and $(\boldsymbol{g}_{k+1}, \boldsymbol{h}_{k+1})$ can be expressed by $(\boldsymbol{p}_k,\boldsymbol{q}_k)$, and we have

$$\begin{aligned} &\begin{bmatrix} \boldsymbol{g}_k \\ \boldsymbol{h}_k \end{bmatrix} = \begin{bmatrix} < \hat{p}_{\alpha k}^{-1-\delta}(\theta_k) > & \boldsymbol{0} \\ \boldsymbol{0} & < \bar{\hat{p}}_{\alpha k}^{-1-\delta}(\theta_k) > \end{bmatrix}\begin{bmatrix} \boldsymbol{B}_k^{\mathrm{T}} & \boldsymbol{A}_k^{\mathrm{T}} \\ \bar{\boldsymbol{B}}_k^{\mathrm{T}} & \bar{\boldsymbol{A}}_k^{\mathrm{T}} \end{bmatrix} \\ &\quad \begin{bmatrix} \boldsymbol{p}_k \\ \boldsymbol{q}_k, \end{bmatrix}, \\ &\begin{bmatrix} \boldsymbol{g}_{k+1} \\ \boldsymbol{h}_{k+1} \end{bmatrix} = \begin{bmatrix} < \hat{p}_{\alpha k+1}^{-1-\delta}(\theta_k) > & \boldsymbol{0} \\ \boldsymbol{0} & < \bar{\hat{p}}_{\alpha k+1}^{-1-\delta}(\theta_k) > \end{bmatrix} \\ &\quad \begin{bmatrix} \boldsymbol{B}_{k+1}^{\mathrm{T}} & \boldsymbol{A}_{k+1}^{\mathrm{T}} \\ \bar{\boldsymbol{B}}_{k+1}^{\mathrm{T}} & \bar{\boldsymbol{A}}_{k+1}^{\mathrm{T}} \end{bmatrix}\begin{bmatrix} \boldsymbol{p}_k \\ \boldsymbol{q}_k \end{bmatrix} \end{aligned} \tag{A3}$$

In the above equation, letting $k = k + 1$ in Eq. $(A3)_1$ and using Eq. (26), we can find the relation between $(\boldsymbol{p}_k,\boldsymbol{q}_k)$ and $(\boldsymbol{p}_{k+1},\boldsymbol{q}_{k+1})$ as

$$\begin{bmatrix} \boldsymbol{p}_k \\ \boldsymbol{q}_k \end{bmatrix} = \hat{\boldsymbol{N}}_{k+1}^{1+\delta}(\theta_k, \theta_{k+1})\begin{bmatrix} \boldsymbol{p}_{k+1} \\ \boldsymbol{q}_{k+1} \end{bmatrix} \tag{A4}$$

Using Eqs. (37) and (21), we have

$$\begin{aligned} &\begin{bmatrix} \boldsymbol{B}_1 & \overline{\boldsymbol{B}}_1 \end{bmatrix}\begin{bmatrix} < \hat{p}_{\alpha 1}^{1+\delta}(\theta_0) > \boldsymbol{0} & \\ \boldsymbol{0} & < \overline{\hat{p}}_{\alpha 1}^{1+\delta}(\theta_0) > \end{bmatrix}\begin{bmatrix} \boldsymbol{g}_1 \\ \boldsymbol{h}_1 \end{bmatrix} = \boldsymbol{0}, \\ &\begin{bmatrix} \boldsymbol{A}_n & \overline{\boldsymbol{A}}_n \end{bmatrix}\begin{bmatrix} < \hat{p}_{\alpha n}^{1+\delta}(\theta_n) > \boldsymbol{0} & \\ \boldsymbol{0} & < \overline{\hat{p}}_{\alpha n}^{1+\delta}(\theta_n) > \end{bmatrix}\begin{bmatrix} \boldsymbol{g}_n \\ \boldsymbol{h}_n \end{bmatrix} = \boldsymbol{0}, \\ &\begin{bmatrix} \boldsymbol{A}_k & \overline{\boldsymbol{A}}_k \\ \boldsymbol{B}_k & \overline{\boldsymbol{B}}_k \end{bmatrix}\begin{bmatrix} < \hat{p}_{\alpha k}^{1+\delta}(\theta_k) > \boldsymbol{0} & \\ \boldsymbol{0} & < \overline{\hat{p}}_{\alpha k}^{1+\delta}(\theta_k) > \end{bmatrix}\begin{bmatrix} \boldsymbol{g}_k \\ \boldsymbol{h}_k \end{bmatrix} \\ &= \begin{bmatrix} \boldsymbol{A}_{k+1} & \overline{\boldsymbol{A}}_{k+1} \\ \boldsymbol{B}_{k+1} & \overline{\boldsymbol{B}}_{k+1} \end{bmatrix}\begin{bmatrix} < \hat{p}_{\alpha k+1}^{1+\delta}(\theta_k) > \boldsymbol{0} & \\ \boldsymbol{0} & < \overline{\hat{p}}_{\alpha k+1}^{1+\delta}(\theta_k) > \end{bmatrix} \end{aligned}$$

$$\begin{bmatrix} \boldsymbol{g}_{k+1} \\ \boldsymbol{h}_{k+1} \end{bmatrix} = \begin{bmatrix} \boldsymbol{p}_k \\ \boldsymbol{q}_k \end{bmatrix} \tag{A5}$$

In Eq. (A3), setting $k = 1$ for $(\boldsymbol{g}_k, \boldsymbol{h}_k)$ and $k = n - 1$ for $(\boldsymbol{g}_{k+1}, \boldsymbol{h}_{k+1})$, we obtain two new equations. Substituting them into Eq. (A5), and together with Eq. (A4), we obtain

$$\begin{bmatrix} \hat{\boldsymbol{N}}_{1L}^{1+\delta}(\theta_0, \theta_1)\prod_{j=2}^{n-1}\hat{\boldsymbol{N}}_j^{1+\delta}(\theta_{j-1}, \theta_j) \\ \hat{\boldsymbol{N}}_{nU}^{1+\delta}(\theta_n, \theta_{n-1}) \end{bmatrix}\begin{bmatrix} \boldsymbol{p}_{n-1} \\ \boldsymbol{q}_{n-1} \end{bmatrix} = \boldsymbol{0} \tag{A6}$$

References

1. Levine D, Steinhardt PJ. Quasicrystals: a new class of ordered structures. Phys Rev Lett. 1984;53(26):2477–80. https://doi.org/10.1103/physrevlett.53.2477.
2. Wang RH, Hu CZ, Gui JN. Quasicrystal physics. Science Press, 2004.
3. Qiao YF, Hou GL, Chen A. Symplectic approach for plane elasticity problems of two-dimensional octagonal quasicrystals. Appl Math Comput. 2021;400(20):1–17. https://doi.org/10.1016/j.amc.2021.126043.
4. Fan TY. Mathematical theory and methods of mechanics of quasicrystalline materials. Engineering.2013;5(4):407–48. https://doi.org/10.4236/eng.2013.54053.
5. Li XY, Li PD, Wu TH, Shi MX, Zhu ZW. Three-dimensional fundamental solutions for one-dimensional hexagonal quasicrystal with piezoelectric effect. Phys Lett A. 2014;378(10):826–34. https://doi.org/10.1016/j.physleta.2014.01.016.
6. Hu CZ, Wang RH, Ding DH, Yang WG. Piezoelectric effects in quasicrystals. Phys Rev B. 1997;56(5):2463–9. https://doi.org/10.1103/PhysRevB.56.2463.
7. Zhang L, Guo JH, Xing YM. Bending analysis of functionally graded one-dimensional hexagonal piezoelectric quasicrystal multilayered simply supported nanoplates based on nonlocal strain gradient theory. Acta Mech Solida Sin. 2021;34(2):237–51.
8. Wang YB, Guo JH. Effective electroelastic constants for three-phase confocal elliptical cylinder model in piezoelectric quasicrystal composites. Appl Math Mech Engl. 2018;39(6):797–812. https://doi.org/10.1007/s10483-018-2336-9.
9. Mu X, Fu XY, Zhang LL, Zhu ZW, Zhang JM, Gao Y. Fundamental solutions of critical wedge angles for one-dimensional piezoelectric quasicrystal wedge. Appl Math Mech Engl. 2022;43(5):709–28. https://doi.org/10.1007/s10483-022-2847-6.
10. Zhang ZG, Ding SH, Li X. A spheroidal inclusion within a 1D hexagonal piezoelectric quasicrystal. Arch Appl Mech. 2020;90(5):1039–58. https://doi.org/10.1007/s00419-020-01657-8.
11. Zhao MH, Dang HY, Fan CY, Chen ZT. Analysis of a three-dimensional arbitrarily shaped interface crack in a one-dimensional hexagonal thermo-electro-elastic quasicrystal bi-material, part 1: theoretical solution. Eng Fract Mech. 2017;179:59–78. https://doi.org/10.1016/j.engfracmech.2017.04.019.
12. Dang HY, Zhao MH, Fan CY, Chen ZT. Analysis of a three-dimensional arbitrarily shaped interface crack in a one-dimensional hexagonal thermo-electro-elastic quasicrystal bi-material, Part 2: numerical method. Eng Fract Mech. 2017;180:268–81. https://doi.org/10.1016/j.engfracmech.2017.05.042.

13. Mu X, Xu WS, Zhu ZW, Zhang LL, Gao Y. Multi-field coupling solutions of functionally graded two-dimensional piezoelectric quasicrystal wedges and spaces. Appl Math Model. 2022;109:251–64. https://doi.org/10.1016/j.apm.2022.04.018.
14. Zhang LL, Wu D, Xu WS, Yang LZ, Ricoeur A, Wang ZB, Gao Y. Green's functions of one-dimensional quasicrystal bi-material with piezoelectric effect. Phys Lett A. 2016;380(39):3222–8. https://doi.org/10.1016/j.physleta.2016.07.043.
15. Chen TH, Chue CH, Lee HT. Stress singularities near the apex of a cylindrically polarized piezoelectric wedge. Arch Appl Mech. 2004;74(3/4):248–61. https://doi.org/10.1016/S0022-3697(98)00081-X.
16. Elliotis MC, Charmpis DC, Georgiou GC. The singular function boundary integral method for an elastic plane stress wedge beam problem with a point boundary singularity. Appl Math Comput. 2014;248:93–100. https://doi.org/10.1016/j.amc.2014.09.090.
17. Xu XL, Rajapakse R. On singularities in composite piezoelectric wedges and junctions. Int J Solids Struct. 2000;37(23):3253–75. https://doi.org/10.1016/S0020-7683(99)00143-2.
18. Wang JS, He XQ, Qin QH. Singularity analysis of electromechanical fields in angularly inhomogeneous piezoelectric composites wedges. IUTAM Symp Multiscale Model Fatigue Damage Fracture Smart Mater. 2011;24:153–61.
19. Chen HP. Stress singularities in anisotropic multi-material wedges and junctions. Int J Solids Struct. 1998;35(11):1057–73. https://doi.org/10.1016/S0020-7683(97)00108-X.
20. Hwu CB, Oomiya M, Kishimoto K. A key matrix for the stress singularity of the anisotropic elastic composite wedges. Jsme Int J. 2003;46(1):40–50. https://doi.org/10.1299/jsmea.46.40.
21. Hwu CB, Ikeda T. Electromechanical fracture analysis for corners and cracks in piezoelectric materials. Int J Solids Struct. 2008;45(22–23):5744–64. https://doi.org/10.1016/j.ijsolstr.2008.0.
22. Hwu CB, Lee WJ. The singularity in multi-material wedges under thermal loading. Key Eng Mater. 2004;4(1):345–50. https://doi.org/10.4028/www.scientific.net/KEM.261-263.345.
23. Hwu CB, Oomiya M, Kishimoto K. Stress singularities of multi-bonded anisotropic wedges. Apcfs Atem. 2001. https://doi.org/10.1299/jsmeatemapcfs.2.01.03.0_740.
24. Chuang WY, Sung JC, Chung WG. Stress singularities of two special geometries of wedges with free-mixed boundary conditions. Comput Struct. 2003;81(3):167–76. https://doi.org/10.1016/S0045-7949(02)00435-2.
25. Fan TY. Mathematical theory of elasticity of quasicrystals and its applications. Science Press, 2011.
26. Ding DH, Yang WG, Hu CZ, Wang RH. Generalized elasticity theory of quasicrystals. Phys Rev B. 1993;48(10):7003–10. https://doi.org/10.1103/PhysRevB.48.7003.
27. Hwu CB.Anisotropic elastic plates. Springer. 2010.
28. Williams ML. Stress singularities resulting from various boundary conditions in angular corners of plates in extension. J Appl Mech. 1952;19:526–8. https://doi.org/10.1007/s11837-015-1764-2.
29. Suo ZG. Singularities,interfaces and cracks in dissimilar anisotropic media.Proc R Soc Lond Ser A Math Phys Sci.1873;1990(427):331–58. https://doi.org/10.1098/rspa.1990.0016
30. Ting TCT. Anisotropic elasticity: theory and applications. Oxford University, 1996.